Eur. Phys. J. C 45, 783–795 (2006)
Digital Object Identifier (DOI) 10.1140/epjc/s2005-02452-1

THE EUROPEAN PHYSICAL JOURNAL C

Lepton-pair production from deep inelastic scattering in peripheral relativistic heavy ion collisions

U. Dreyer, T. Baier, K. Hencken, D. Trautmann

Institute of Physics, University of Basel, Klingelbergstr. 82, 4056 Basel, Switzerland

Received: 8 August 2005 / Revised version: 28 October 2005 /
Published online: 21 December 2005 –

Abstract. We calculate the inelastic electron- and muon-pair production in peripheral relativistic heavy ion collisions in the region of large Q^2 of one of the photons. This offers a possibility to study the quark distribution functions in ions in "ultraperipheral heavy ion collisions". The calculations are compared with those making use of the equivalent photon and the equivalent lepton approximation. We compare the results for Pb–Pb and Pb–p collisions at RHIC ($\gamma \approx 100$) and LHC ($\gamma \approx 3000$) energies. Furthermore we include nuclear modifications to the parton distribution functions in our calculations to study their effect on the cross sections.

1 Introduction

In heavy ion collisions the electromagnetic production of lepton pairs has a large cross section and has to be considered as important background [1]. The dominant process for pair creation is the two-photon process. Up to now predominantly those processes with two coherent interactions at the nuclei, given by $Q^2 \leq \frac{1}{R^2}$ (with $Q^2 = -q^2$ and where R is the size of the nucleus), which are enhanced by a factor Z^4, have been considered, for example in [1–4]. There is another class of processes, which are much rarer, where one of the interactions is coherent and the other involves a deep inelastic scattering ($Q^2 \geq \frac{1}{R^2}$); see Fig. 1.

The Feynman diagram of the two-photon pair production process in heavy ion collisions has three internal lines, two photons (see Fig. 1) and one lepton (see Fig. 2). Large contributions to the matrix element are always associated with small denominators of the corresponding propagators, which corresponds to almost on-shell intermediate particles. Since in the two-photon pair production at most two virtual particles can become almost on-shell at the same time, we have two kinematical regions that contribute: the double photon-pole region and the photon–lepton-pole region, where one photon and the intermediate lepton are almost on-shell [5]. For small transverse momenta of the leptons, the double photon-pole region gives the dominant contribution. But as soon as we select events with at least one lepton with large transverse momentum, the two contributions become comparable in size but have different event characteristics. Whereas in the double photon-pole contribution the two leptons are produced back to back in the transverse plane, that is with the same transverse momentum, in the lepton-pole contribution only one of the leptons obtains a large transverse momentum. In this contribution the large transverse momentum comes from a large momentum transfer Q^2 of the off-shell photon, which guarantees the applicability of the parton model in this case. For a detailed discussion and approximate numerical results of both contributions we refer to [6].

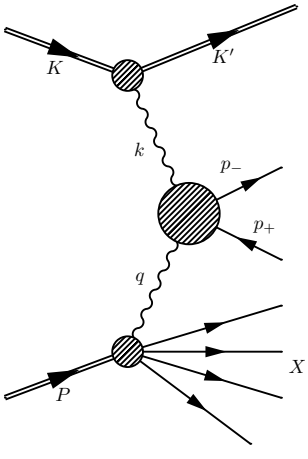

Fig. 1. Schematic Feynman diagram for the inelastic pair production in heavy ion collisions in lowest order

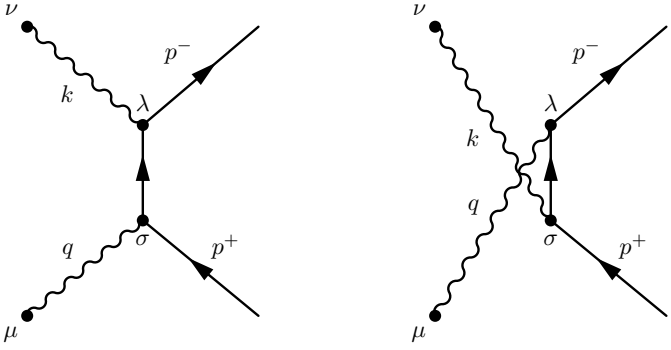

Fig. 2. Lowest order Feynman diagrams for two-photon pair production

The asymmetry in the angular distribution of the leptons, together with the break-up of only one of the nuclei and the potential observation of the corresponding parton jet, is characteristic for the kind of pair production process, we study here, with one coherent and one deep inelastic interaction. Therefore this unique event characteristic offers a possibility to differentiate between the deep inelastic scattering and potential background, such as the doubly coherent process, which yields a more symmetric distribution of the produced leptons.

In this paper we aim to study in which kinematical region one could expect a viable amount of events of the described characteristics and the feasibility to study the structure of nuclei from these processes.

The cross section of the pair production to leading order in a plane wave approximation is elaborated in Sect. 2.

A related process, namely a real photon that produces a lepton pair by inelastic scattering, was calculated by Drell and Walecka in [7] with the aim to study nuclear excitation and in [6], where the production of muon pairs at large transverse momenta is studied.

As already discussed above, due to the $\frac{1}{k^2}$-dependence of the photon propagator, the largest contributions come from the region, where the photon, which is emitted elastically, is almost real, and it was shown in [8–10], that in such situations the equivalent photon approximation can be applied. The process then reduces to the one studied in [7] folded with the equivalent photon spectrum.

A second propagator whose denominator might become small, is the intermediate lepton propagator. Therefore we expect large contributions from the region, where the intermediate lepton is almost on-shell. In such a situation the equivalent lepton approximation, as described in [5,11], should be applicable. Taken together the two approximations simplify the calculation quite considerably and provide handy expressions. This approximation would therefore be very useful also for processes similar to the one studied here and has already been used before [6]. It is therefore of interest to test the validity of these approximations.

In addition, the equivalent lepton approximation provides a simple interpretation of the process, studied here, in terms of the parton picture, because one of the leptons can be related directly to the deep inelastic scattering, whereas the other acts as spectator in accordance with the event characteristics described above.

Apart from these simplifications a further advantage of the equivalent particle approximations is that in them an impact parameter smaller than $R_1 + R_2$ (assuming equal nuclei $b < 2R$), where the nuclei interact strongly, can be excluded, which is not done in the plane wave approach used here for the full calculation. Our calculated cross sections are in this respect an upper limit to the real ones. But we do not expect the deviation to be very large, because the virtuality of the other photon k^2 is small and therefore the impact parameter will most likely be large.

We introduce the equivalent particle spectra in Sect. 3 and carry out their application to the process under consideration. In Sect. 4 we present results for the differential cross sections for all three calculations as well as the calculations including nuclear modifications, compare them and discuss the results.

Throughout this paper we set $\hbar = c = 1$ and use Heaviside–Lorentz units with $e^2 = 4\pi\alpha$.

2 Lepton-pair production

In this section we derive the two-photon pair production process in relativistic heavy ion collisions in a general formulation. The whole process is depicted in Fig. 1, where the circle in the middle stands for the two Feynman diagrams that contribute in lowest order quantum electrodynamics to the matrix element of the two-photon pair production; see Fig. 2. From these two diagrams we obtain the invariant amplitudes [12,13]

$$\mathcal{M}_{1\mu\nu} = e^2 \frac{1}{k^2} \frac{1}{q^2} \left[\bar{u}(p_-)\gamma_\mu \frac{\not{k} - \not{p}_+ + m}{(k-p_+)^2 - m^2} \gamma_\nu v(p_+) \right], \tag{1}$$

$$\mathcal{M}_{2\mu\nu} = e^2 \frac{1}{k^2} \frac{1}{q^2} \left[\bar{u}(p_-)\gamma_\nu \frac{\not{p}_- - \not{k} + m}{(p_- - k)^2 - m^2} \gamma_\mu v(p_+) \right]. \tag{2}$$

Here q and k are the momenta of the photons, p_- and p_+ denote the momenta of the produced leptons and m is the lepton mass. We obtain the matrix element for lepton-pair production as the coherent sum of the two amplitudes

$$M_{\mu\mu'\nu\nu'} = \sum_{s_-,s_+} \left(\mathcal{M}_{1\mu\nu} + \mathcal{M}_{2\mu\nu}\right)\left(\bar{\mathcal{M}}_{1\mu'\nu'} + \bar{\mathcal{M}}_{2\mu'\nu'}\right). \tag{3}$$

Performing the spin summation leads to the usual traces of Dirac γ-matrices:

$$\begin{aligned} M_{\mu\mu'\nu\nu'} = \frac{e^4}{q^4k^4} \Bigg\{ & \frac{1}{x_2^2} \mathrm{Tr}\left(\gamma_{\nu'}(\not{k} - \not{p}_+ + m)\gamma_{\mu'}(\not{p}_- + m)\gamma_\mu \right. \\ & \left. \times (\not{k} - \not{p}_+ + m)\gamma_\nu(\not{p}_+ - m)\right) \\ & + \frac{1}{x_1x_2} \mathrm{Tr}\left(\gamma_{\nu'}(\not{k} - \not{p}_+ + m)\gamma_{\mu'}(\not{p}_- + m)\gamma_\nu \right. \\ & \left. \times (\not{p}_- - \not{k} + m)\gamma_\mu(\not{p}_+ - m)\right) \\ & + \frac{1}{x_1x_2} \mathrm{Tr}\left(\gamma_{\mu'}(\not{p}_- - \not{k} + m)\gamma_{\nu'}(\not{p}_- + m)\gamma_\mu \right. \\ & \left. \times (\not{k} - \not{p}_+ + m)\gamma_\nu(\not{p}_+ - m)\right) \\ & + \frac{1}{x_1^2} \mathrm{Tr}\left(\gamma_{\mu'}(\not{p}_- - \not{k} + m)\gamma_{\nu'}(\not{p}_- + m)\gamma_\nu \right. \\ & \left. \times (\not{p}_- - \not{k} + m)\gamma_\mu(\not{p}_+ - m)\right) \Bigg\}, \end{aligned} \tag{4}$$

where x_1 and x_2 are the negative of the denominators of the lepton propagators

$$-x_1 = (p_- - k)^2 - m^2 = k^2 - 2p_- \cdot k, \tag{5}$$

$$-x_2 = (k - p_+)^2 - m^2 \;=\; k^2 - 2p_+ \cdot k\,. \tag{6}$$

The total cross section is given by

$$\begin{aligned}\sigma_{PK\to P'K'p_+p_-} &= \frac{Z^4\,(4\pi\alpha)^4}{F}\\ &\times \int (2\pi)^4\delta^4(P + K - P' - K' - p_+ - p_-)\,|T|^2\\ &\times \frac{\mathrm{d}^3p_+}{(2\pi)^3 2\epsilon_+}\;\frac{\mathrm{d}^3p_-}{(2\pi)^3 2\epsilon_-}\\ &\times \prod_{n_1=1}^{N_1}\frac{\mathrm{d}^4P_{n_1}}{(2\pi)^4}(2\pi)\delta(P_{n_1}^2 - M_{n_1}^2)\delta^4\left(P' - \sum_{n_1}P_{n_1}\right)\\ &\times \prod_{n_2=1}^{N_2}\frac{\mathrm{d}^4K_{n_2}}{(2\pi)^4}(2\pi)\delta(K_{n_2}^2 - M_{n_2}^2)\delta^4\left(K' - \sum_{n_2}K_{n_2}\right),\end{aligned} \tag{7}$$

with F being the flux of the incoming particles. In the inelastic case P' denotes the total momentum of all particles that emerge from the incident proton or ion with momentum P and $|T|^2$ is defined by

$$|T|^2 = \frac{1}{q^4}\,\frac{1}{k^4}\,\Gamma_P^{\mu}\Gamma_P^{\mu'*}\Gamma_K^{\nu}\Gamma_K^{\nu'*}M_{\mu\mu'\nu\nu'}, \tag{8}$$

where Γ_i are the electromagnetic transition currents and $M_{\mu\mu'\nu\nu'}$ as given in (4). The electromagnetic currents can be rephrased in terms of the electromagnetic tensors $W^{\mu\mu'}$ or $W^{\nu\nu'}$, respectively, that describe the inclusive ionic vertices in their most general form, see e.g. [14],

$$\begin{aligned}W^{\mu\mu'} \;&=\; \frac{(2\pi)^4}{(2\pi)(2M_P)}\int \Gamma^{\mu}\Gamma^{\mu'*}\delta^4\left(P - q - \sum_{n_1}P_{n_1}\right)\\ &\times \prod_{n_1=1}^{N_1}\frac{\mathrm{d}^3P_{n_1}}{(2\pi)^3 2E_{n_1}}\;.\end{aligned} \tag{9}$$

The electromagnetic tensors $W^{\mu\mu'}$ and $W^{\nu\nu'}$ can be expressed in terms of two scalar functions W_1 and W_2:

$$\begin{aligned}W^{\mu\mu'} &= W_{1P}\left(-g^{\mu\mu'} + \frac{q^{\mu}q^{\mu'}}{q^2}\right)\\ &+\frac{W_{2P}}{M_P^2}\left(P^{\mu} - \frac{P\cdot q}{q^2}q^{\mu}\right)\left(P^{\mu'} - \frac{P\cdot q}{q^2}q^{\mu'}\right)\end{aligned} \tag{10}$$

and similarly with $q \to k$ and $P \to K$ for $W^{\nu\nu'}$. The contraction $\mathcal{MWWW} = \mathcal{M}_{\mu\mu'\nu\nu'}\mathcal{W}^{\mu\mu'}\mathcal{W}^{\nu\nu'}$ can be expressed through the functions $W_{1,2}$ and eleven independent scalar products of the momenta of the participating particles. We choose these scalar products to be x_1 and x_2, see (5) and (6) above, and

$$\begin{aligned}&x_3 = \frac{K\cdot q}{M_K},\;\; x_4 = \frac{K\cdot \Delta}{M_K},\;\; x_5 = \frac{P\cdot k}{M_P},\;\; x_6 = \frac{P\cdot \Delta}{M_P},\\ &x_7 = \frac{P\cdot K}{M_P M_K},\;\; x_8 = \frac{K\cdot k}{M_K},\;\; x_9 = k^2,\;\; x_{10} = \frac{P\cdot q}{M_P},\\ &x_{11} = q^2,\end{aligned} \tag{11}$$

with $\Delta = p_- - p_+$. The calculation of the invariant amplitude $\mathcal{MWWW}$ was tested by reproducing the results in [7], where one of the photons is real.

Equation (10) gives the general form of the electromagnetic tensor $W^{\mu\mu'}$ in terms of the two scalar functions W_1 and W_2, which are functions of the two scalar variables q^2 and $\nu_q = -\frac{P\cdot q}{M_P}$ for inclusive processes. Different processes are then described by the use of different forms for W_1 and W_2.

For an elastic interaction at the vertex, we have

$$\nu_q = -\frac{q^2}{2M_P}\,. \tag{12}$$

This means that in the elastic case the $W_{1,2}$ depend on one of the scalars q^2 and ν_q only. The main contribution to the integral in the elastic case comes from the region of small q^2 because of the $\frac{1}{q^4}$-dependence of the invariant amplitude and it is therefore a good approximation to set $\nu_q = 0$, which means neglecting the recoil. The structure functions $W_{1,2}$ are then given by

$$W_1 = 0, \qquad W_2 = |F(q^2)|^2\delta\left(\nu_q\right), \tag{13}$$

where we choose the form factor $F(q^2)$ for ions as

$$F(q^2) = \exp\left(\frac{q^2}{2Q_0^2}\right), \tag{14}$$

with $Q_0 = 60\,\mathrm{MeV}$.

The pair production cross section for elastic interaction of both ions is calculated as a test and found to be in good agreement with e.g. the formula given by Racah [2] and results from [3], respectively.

Our intention is to perform the calculation of the cross section for lepton-pair production in deep inelastic scattering. To this purpose we use the parton model, see e.g. [15], to express the structure functions for protons in deep inelastic scattering in terms of the parton distribution functions. For protons we have

$$W_1 \;=\; \frac{1}{2M_p x}F_2^p(x), \qquad W_2 \;=\; \frac{2M_p x}{Q^2}F_2^p(x), \tag{15}$$

where F_2^p is the structure function of the proton:

$$F_2^p(x) = \sum_{i=q\bar{q}} e_i^2 x f_i(x)\,. \tag{16}$$

The scaling variable x denotes the fraction of the proton momentum of the struck parton in the infinite momentum frame and is also equal to the kinematic quantity $\frac{Q^2}{2M_p\nu_q}$, where M_p is the proton mass and e_i denotes the fraction of the elementary charge of parton i. We take the parton distribution functions for the proton from Cteq61 [16].

Assuming that the parton distribution functions for the neutron correspond to the ones for the proton, if we exchange the u- with the d-quark, $f^n_{u(\bar{u})} = f^p_{d(\bar{d})}$ and $f^n_{d(\bar{d})} = f^p_{u(\bar{u})}$, we can calculate the ion collision case using

$$F_2^A\left(x\right) = Z\cdot F_2^p(x) + (A - Z)\cdot F_2^n(x) \tag{17}$$

instead of F_2^p, which means we consider the nucleons as partons of the ion carrying a momentum fraction $\frac{1}{A}$, where A denotes the mass number of the nucleus.

Nuclear effects, such as nuclear shadowing, antishadowing etc., affect the parton distribution functions (PDFs) of nucleons that are bound in a nucleus. The differences between free PDFs and nuclear PDFs can be accounted for by multiplying the free PDFs by flavor dependent factors

$$f_i^{p|A}(x,Q^2) = R_i(x,Q^2) \cdot f_i^p(x,Q^2)\,. \tag{18}$$

For small Q^2, which is the region we are interested in, two parameterizations are given by Eskola et al. in [17,18] and Frankfurt et al. in [19,20].

There are non-trivial restrictions on the phase space, e.g. $(k+q)^2$ cannot be smaller than $4m^2$ for the pair production process to be possible. As these restrictions are complicated to implement efficiently into the numerical integration, we describe the phase space by a set of variables given in [21], where the final particle phase space is split into a chain of successive two particle decays. We integrate over the invariant masses of the intermediate states and the angles in the center of momentum system of the decaying particle. The momenta generated by the integration variables have then to be transformed into one common system. We choose this system to be the center of momentum system of the two colliding ions.

3 The equivalent photon and lepton approximation

As already discussed in the introduction, two kinematical regions contribute to the production of leptons with large transverse momenta. There is the first region of the double photon-pole, where both photons are quasireal, and the leptons are produced back to back with about equal transverse momenta.

In this paper we are mainly concerned with the second region, the photon–lepton-pole region, where one of the photons as well as the intermediate lepton are almost on-shell. In this kinematical region one lepton is produced with large transverse momentum, whereas the transverse momentum of the second lepton is comparatively small. The photon–lepton-pole not only leads to an unique event characteristic, but can also be treated in an approximation, which on the one hand simplifies the cross section calculation quite considerably, and on the other hand provides a simple interpretation of the process in terms of a parton picture.

The parton model, which was already used in Sect. 2 to describe the deep inelastic scattering, can be extended to photons and leptons. In the same way as nuclei consist of nucleons that in turn consist of quarks and gluons, electrons are composed of photons, that in turn have leptons as constituents.

Due to the coherent action of all the charges in the nucleus, relativistic nuclei have photons as important constituents. The coherence condition limits the virtuality of the photon to $-k^2 \leq \frac{1}{R^2}$, that means the wavelength of the photon is larger than the nucleus and does not resolve individual nucleons. This is the case for the elastic part of the process $A_P A_K \longrightarrow X A_{K'} l^+ l^-$. Therefore we can apply the equivalent photon approximation (EPA), introduced by Weizsäcker and Williams in [22,23] as well as by Fermi in [24]. For a detailed discussion of applications of this approximation in heavy ion collisions see [1,8–10]. In this approximation this kind of processes can be written as a convolution of the equivalent photon spectrum of the incident particle and the real photon process (see Fig. 3):

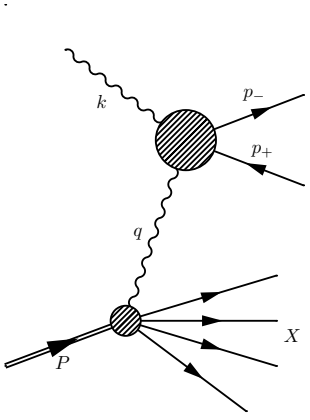

Fig. 3. Inelastic lepton-pair production by a real photon on a nucleus as used in the equivalent photon approximation

$$\sigma_{AA \longrightarrow AXl^+l^-} = \int \mathrm{d}u f_{\gamma|A}(u) \sigma_{\gamma A \longrightarrow Xl^+l^-}(\omega)\,. \tag{19}$$

The photons are considered to be emitted in forward direction with energy $\omega = u \cdot E_K$, where E_K is the energy of the incident ion. $f_{\gamma|A}$ is the structure function for the distribution of photons in the ion. We use the approximation

$$f_{\gamma|A}(u) = \frac{2\alpha}{\pi} \frac{Z^2}{u} \ln\left(\frac{1}{uM_K R}\right)\,. \tag{20}$$

The maximal value of u is restricted by the coherence condition to $u \leq \frac{1}{M_K R}$ which is $\approx 1.4 \cdot 10^{-4}$ for Pb.

$f_{\gamma|A}(u)$ has to be folded with the pair production cross section by a real and a virtual photon as shown in Fig. 3.

A further simplification can be achieved by treating the intermediate lepton as quasireal as well, assuming photon-splitting into an almost collinear lepton pair. The spectrum of equivalent leptons in the photon can be derived from the matrix element of the lepton photon vertex, assuming small transverse momenta of the emitted particles and high energies. The equivalent lepton spectrum is given in [5,11] as

$$f_{l|\gamma}(\omega,z) = \frac{\alpha}{\pi} \ln\left(\frac{\omega}{m}\right)\left[z^2 + (1-z)^2\right], \tag{21}$$

where m is the mass, $E_l = z \cdot \omega$ the energy of the lepton and ω the energy of the photon. The total number of equivalent leptons in the ion K can be derived from the convolution of the two spectra:

$$f_{l|A}(w) = \int_w^{1/RM_K} \frac{\mathrm{d}u}{u} f_{\gamma|A}(u) f_{l|\gamma}\left(\omega = u \cdot E_K, z = \frac{w}{u}\right), \tag{22}$$

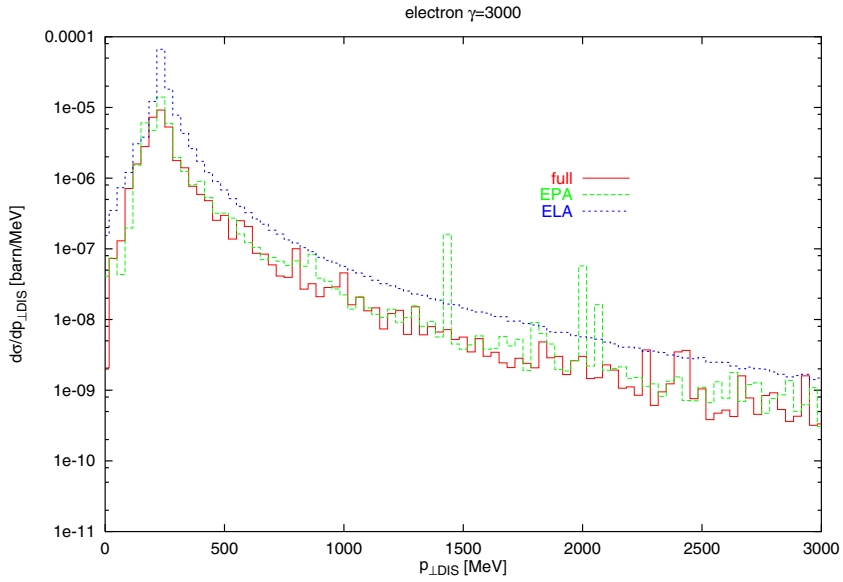

Fig. 4. Differential cross section as a function of the transverse momentum of the "DIS lepton" $\frac{\mathrm{d}\sigma}{\mathrm{d}p_{\perp\mathrm{DIS}}}$ for electron-pair production in a Pb–p collision for $\gamma = 3000$ in the full calculation, the EPA, and the ELA

where $w = z \cdot u$ is the fraction of the incident ion energy carried away by the lepton $E_l = w \cdot E_K$.

The leptons can be treated as an equivalent particle beam interacting with the target via deep inelastic scattering. For the total cross section the equivalent lepton spectrum of the ion $f_{l|A}(w)$ has to be folded with the cross section of lepton–proton deep inelastic scattering, which can be found in the literature, e.g. [15], and the total cross section is then given by

$$\sigma_{AA\longrightarrow\ AXl_+l_-} = \int_{m/E_K}^{1/RM_K} \mathrm{d}w f_{l|A}(w)\sigma_{lA\longrightarrow\ l'X}\ . \quad (23)$$

Because of the $\ln\left(\frac{\omega}{m}\right)$-dependence of the equivalent lepton spectrum, this two-step approximation is no longer Lorentz invariant. Especially for muon-pair production the cross sections are sensitive to the Lorentz frame chosen. Since the equivalent lepton spectrum, given in [5], is derived in the infinite momentum frame, the target system, where the energy of the incoming ion is $(2\gamma^2-1)M_K$ instead of γM_K, seems to be the appropriate system and is used throughout the rest of the paper.

4 Results

In the picture of the equivalent lepton approximation one of the produced leptons is directly related to the deep inelastic scattering, whereas the spectator lepton is found in forward direction. If we apply this picture also to the full calculation and the EPA, we can distinguish the two leptons by their transverse momentum, where we consider the "spectator lepton" to have a smaller transverse momentum. By this means we can compare the results of the full calculation and the EPA with those of the ELA and also give a simple interpretation of the process.

We present differential cross sections as a function of the transverse momenta of the leptons and the struck quark, the scaling variable x of the struck quark within the proton (Pb–p) and the rapidity of the lepton related to the deep inelastic scattering (further referred to as "DIS lepton") and quark for Pb–p and Pb–Pb collisions at two different energies ($\gamma = 100$ and $\gamma = 3000$).

In Fig. 4 we show the differential cross section as a function of the transverse momentum of the "DIS lepton" for electron-pair production in a Pb–p collision at $\gamma = 3000$. We see that the $p_\perp$-criterion for the distinction of the two leptons for the EPA and the full calculation is reasonable, as the shape of these cross sections resembles that of the ELA, where we have only one lepton, the one from the deep inelastic scattering, whereas the second one is assumed to be found at small angles.

In Fig. 5 we compare the differential cross sections as a function of the transverse momenta of both leptons and of the struck quark for the full calculation for electron-pair production at $\gamma = 3000$. At large $p_\perp$ the "spectator lepton" distribution is an order of magnitude smaller than the distribution of the "DIS lepton", which in addition is balanced by the quark transverse momentum distribution. This reflects the event characteristic, which uniquely identifies the pair production with one coherent and one incoherent interaction.

A comparison of the differential cross sections as a function of the transverse momentum of the "DIS lepton" for electron- and muon-pair production in a Pb–p and a Pb–Pb collision is presented in Fig. 6 for $\gamma = 3000$. For transverse momenta larger than $\approx 0.6\,\mathrm{GeV}$ electron- and muon-pair production have similar cross sections and are therefore of equal interest.

We want to investigate the behavior of the approximations for high transverse momenta because this is the interesting region for experiments. Therefore we calculate differential cross sections with the additional constraint that the quark transverse momentum should be larger than $2\,\mathrm{GeV}$ ($p_{\perp\mathrm{quark}} > 2\,\mathrm{GeV}$). We apply the cut on the quark transverse momentum, because it is always related to the high virtuality photon, not depending on the validity of

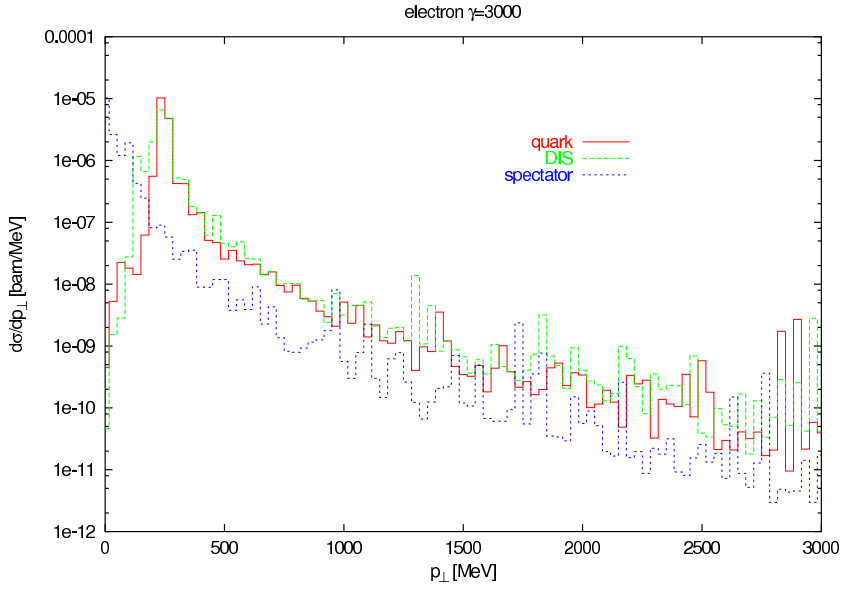

Fig. 5. Comparison between the differential cross section as a function of the transverse momenta $\frac{d\sigma}{dp_\perp}$ of the "spectator lepton", the "DIS lepton" and the struck quark for electron-pair production in a Pb–p collision for $\gamma = 3000$ in the full calculation

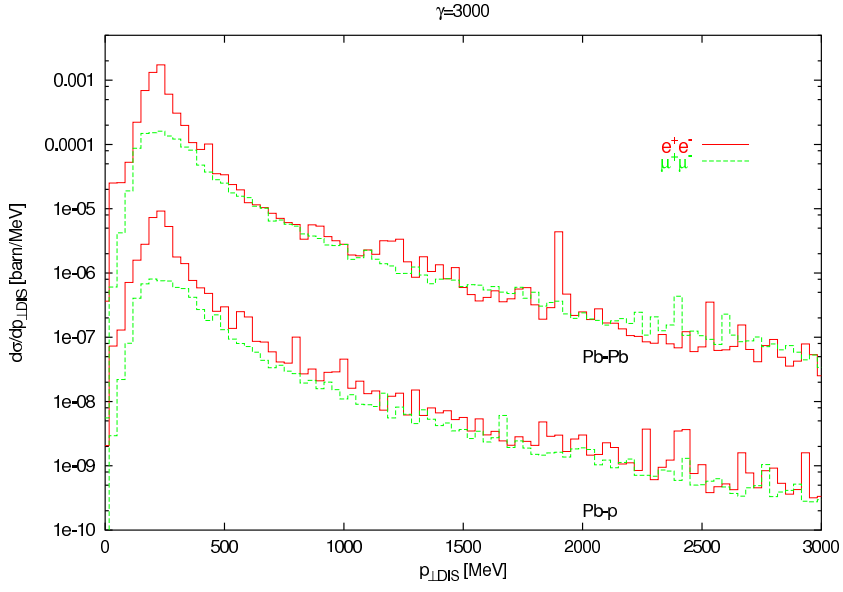

Fig. 6. Comparison between the differential cross sections as a function of the transverse momentum of the "DIS lepton" $\frac{d\sigma}{dp_{\perp\mathrm{DIS}}}$ for electron-pair production in a Pb–p and Pb–Pb collision, for muon-pair production in Pb–p and Pb–Pb collisions for $\gamma = 3000$ in the full calculation

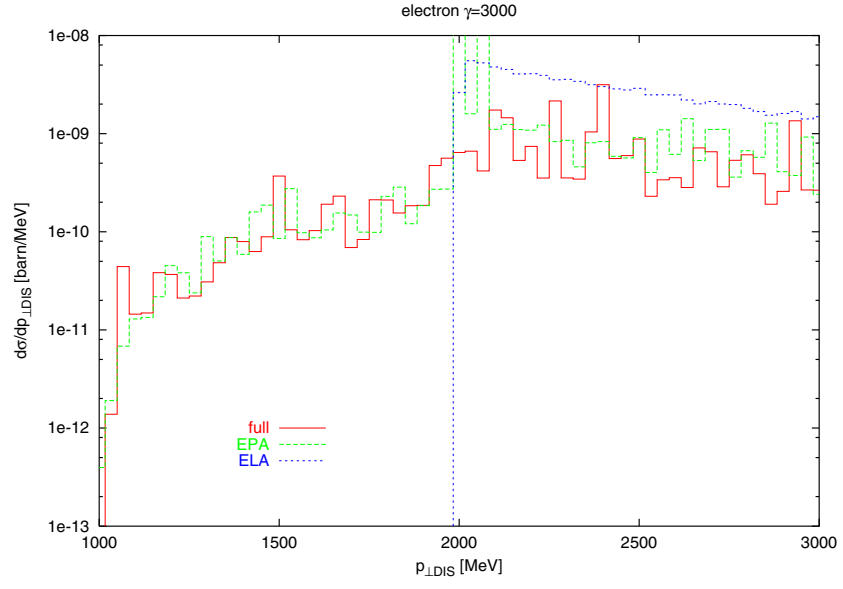

Fig. 7. Same as Fig. 4 with the additional constraint $p_{\perp\mathrm{quark}} > 2\,\mathrm{GeV}$

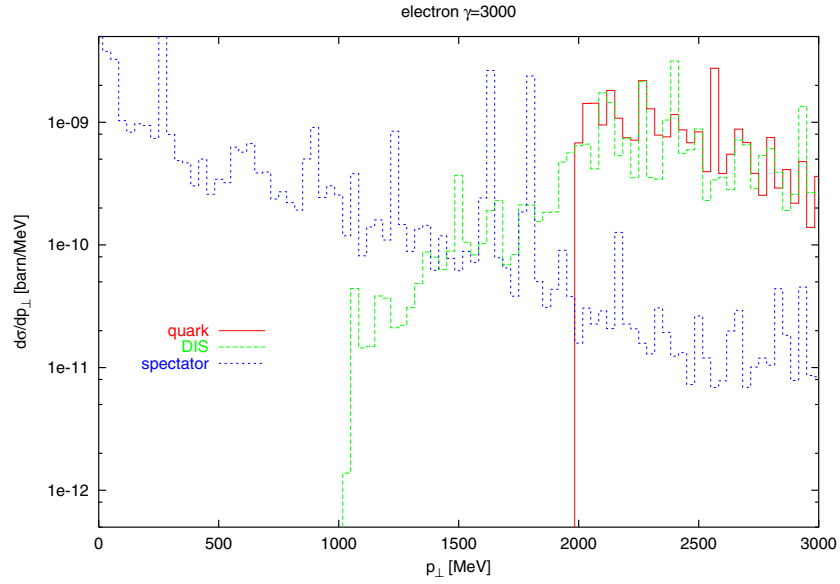

Fig. 8. Same as Fig. 5 with the additional constraint $p_{\perp\mathrm{quark}} > 2\,\mathrm{GeV}$

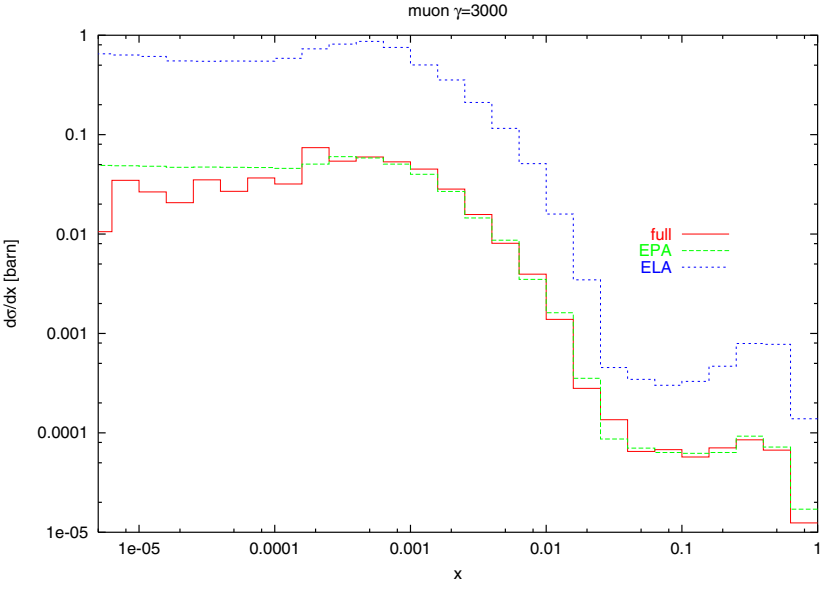

Fig. 9. Differential cross section as a function of the Bjorken scaling variable x of the quark within the proton $\frac{\mathrm{d}\sigma}{\mathrm{d}x}$ for muon-pair production in a Pb–p collision for $\gamma = 3000$ for all three calculations

the "equivalent lepton picture". Fig. 7 is then the same as Fig. 4 with the additional constraint $p_{\perp\mathrm{quark}} > 2\,\mathrm{GeV}$.

The quark transverse momentum cut can also be applied to the comparison of the transverse momenta of the two leptons and the quark in the full calculation, which leads to the distributions in Fig. 8.

In Fig. 9 we show the differential cross section as a function of the Bjorken variable x for muon-pair production in a Pb–p collision for $\gamma = 3000$ for all three calculations. In the infinite momentum frame x denotes the fraction of the proton momentum that is carried by the struck quark.

Fig. 10 shows the differential cross section as a function of x for muon-pair production at $\gamma = 3000$ in a Pb–Pb collision. In these calculations nuclear effects on the parton distribution functions are not taken into account. Fig. 11 is the same as Fig. 9 but again with a $p_{\perp\mathrm{quark}}$-cut at 2 GeV.

In Fig. 12 we present differential cross sections as a function of the rapidity of the "DIS lepton" for muon-pair production at $\gamma = 100$ in a Pb–p collision. The arrows mark the rapidities of the incoming particles (proton and ion).

The differential cross section as a function of the rapidity of the struck quark for muon-pair production at $\gamma = 3000$ in a Pb–p collision can be seen in Fig. 13.

Figs. 14 and 15 show the same as 12 and 13 with the additional constraint $p_{\perp\mathrm{quark}} > 2\,\mathrm{GeV}$.

An important question concerns the actual rate of events in different regions of Q^2 and x. In Figs. 16 and 17 we present the cross section in barn for electron- (Fig. 16) and muon- (Fig. 17) pair production in a Pb–Pb collision for $\gamma = 3000$ as a function of Bjorken x and virtuality of the photon Q^2. Together with the luminosity of $4.2 \times 10^{26}\,\mathrm{cm}^{-2}\mathrm{s}^{-1}$ for Pb at the LHC, which means a cross section of $4.2 \cdot 10^2$ barn corresponds to one event/s, one can make an estimate of how many events and therefore what accuracy one could expect in each kinematical region. From Figs. 16 and 17 we would expect at most about 600 events

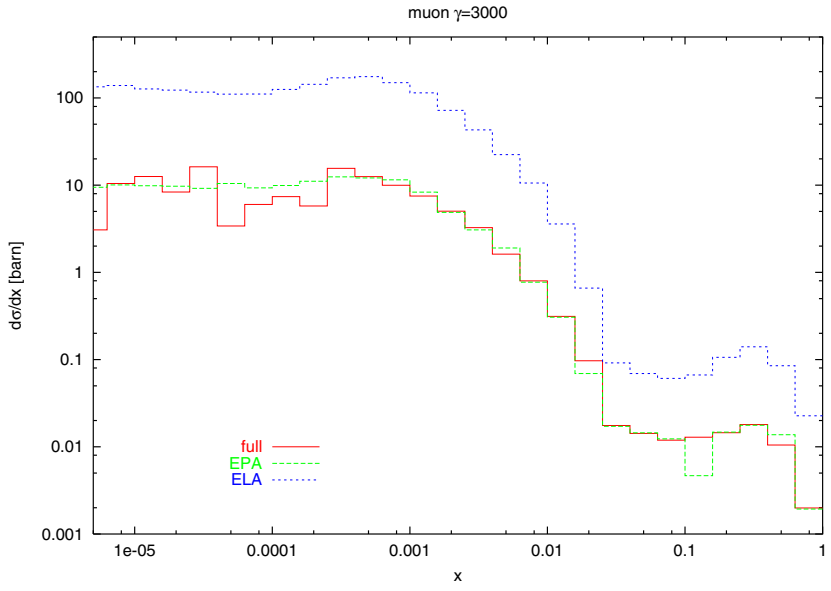

Fig. 10. Differential cross section as a function of the scaling variable x of the quark within the nucleon in the ion $\frac{\mathrm{d}\sigma}{\mathrm{d}x}$ for muon-pair production in a Pb–Pb collision for $\gamma = 3000$ for all three calculations

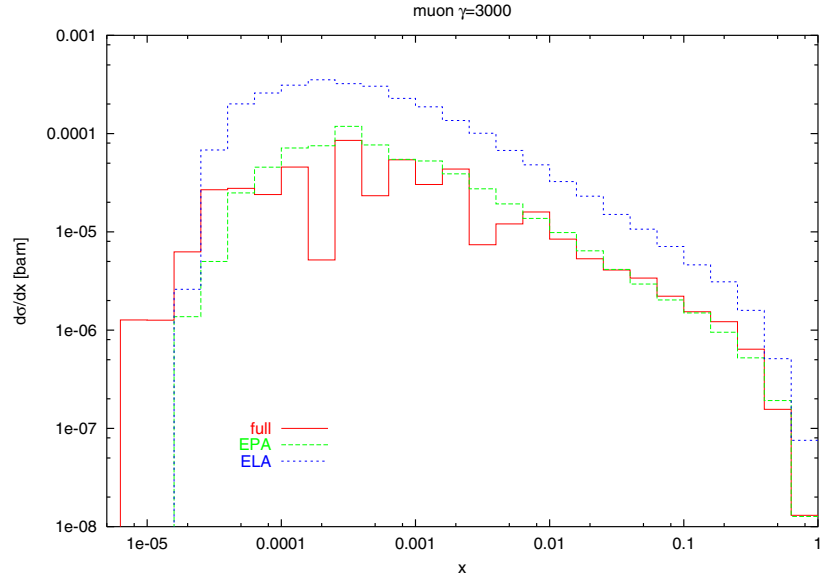

Fig. 11. Same as Fig. 9 with the additional constraint $p_{\perp\mathrm{quark}} > 2\,\mathrm{GeV}$

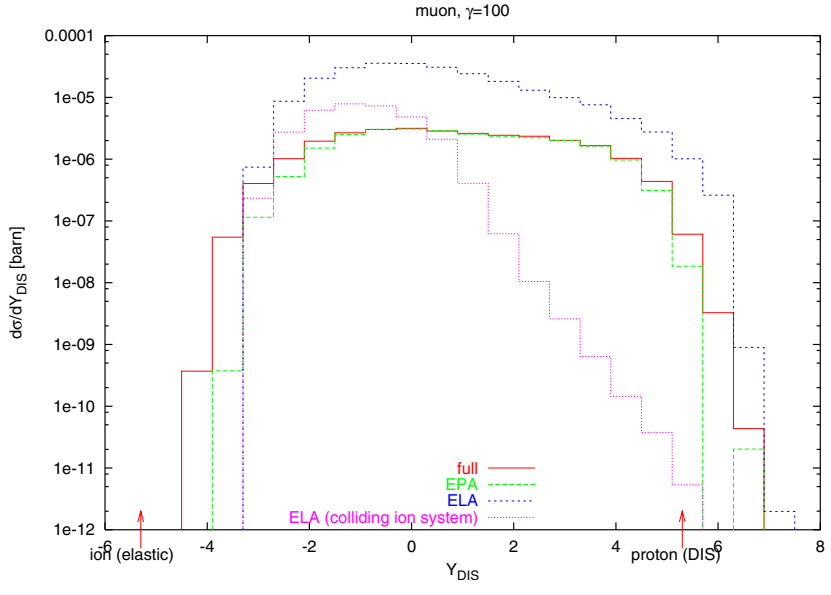

Fig. 12. Differential cross section as a function of the rapidity of the "DIS lepton" $\frac{\mathrm{d}\sigma}{\mathrm{d}Y_{\mathrm{DIS}}}$ for muon-pair production in a Pb–p collision at $\gamma = 100$ in the full calculation, the EPA, and the ELA in the "target system" and in the "colliding ion system"

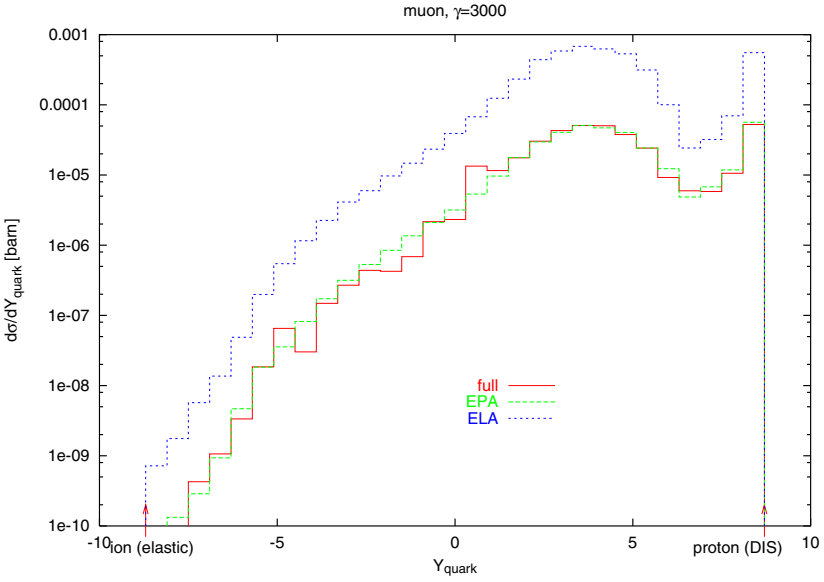

Fig. 13. Differential cross section as a function of the rapidity of the struck quark $\frac{\mathrm{d}\sigma}{\mathrm{d}Y_{\mathrm{quark}}}$ for muon- pair production in a Pb–p collision at $\gamma = 3000$ for all three calculations

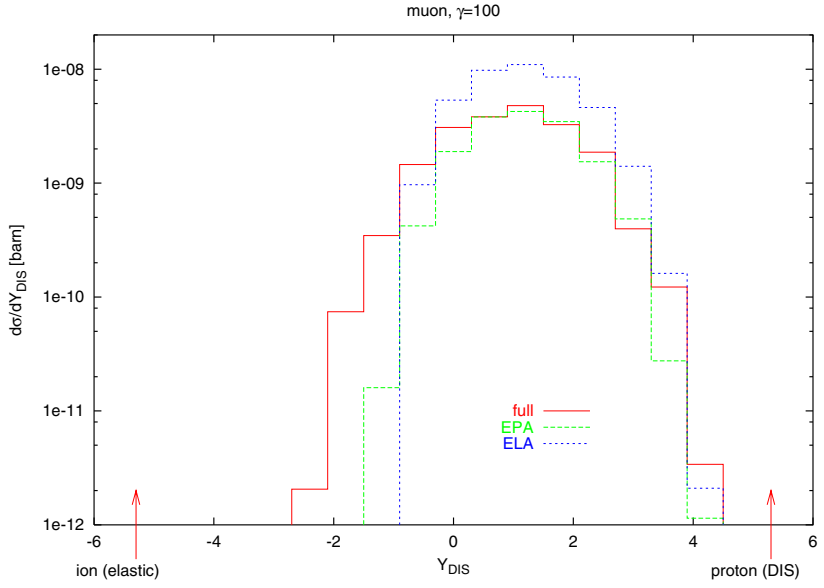

Fig. 14. Same as Fig. 12 with the additional constraint $p_{\perp\mathrm{quark}} > 2\,\mathrm{GeV}$ and without the ELA calculation in the "colliding ion system"

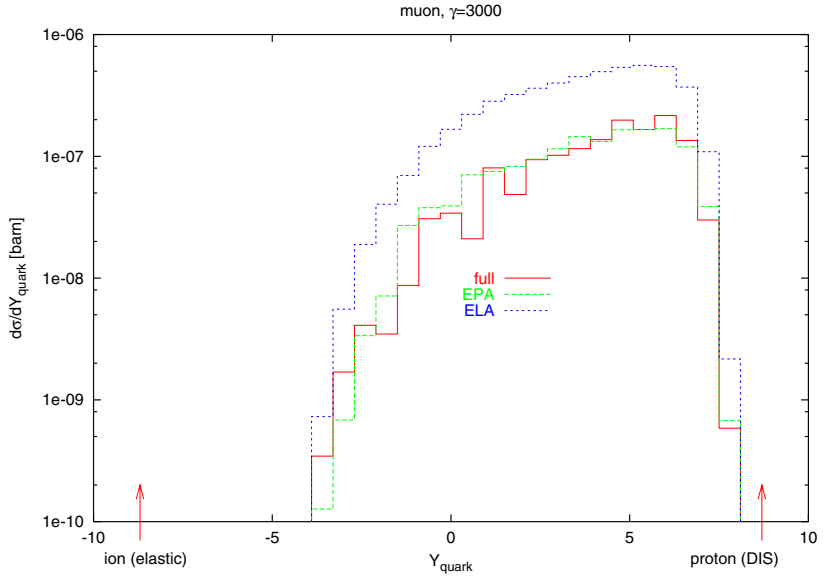

Fig. 15. Same as Fig. 13 with the additional constraint $p_{\perp\mathrm{quark}} > 2\,\mathrm{GeV}$

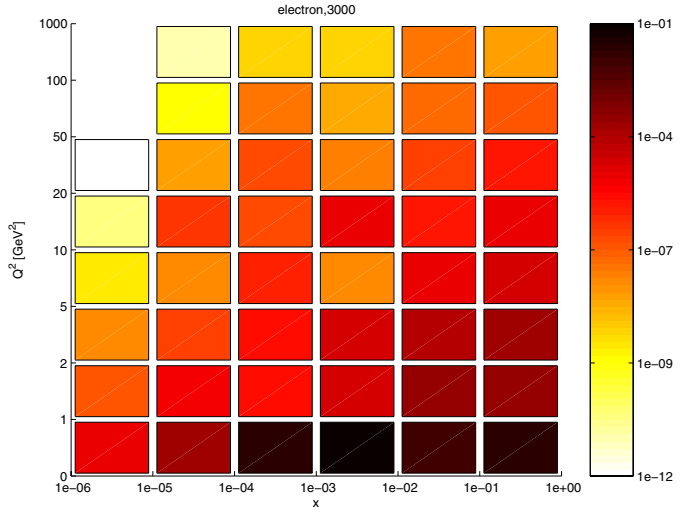

Fig. 16. Cross section in barn as a function of Bjorken x and virtuality of the photon Q^2 for electron-pair production in a Pb–Pb collision at $\gamma = 3000$

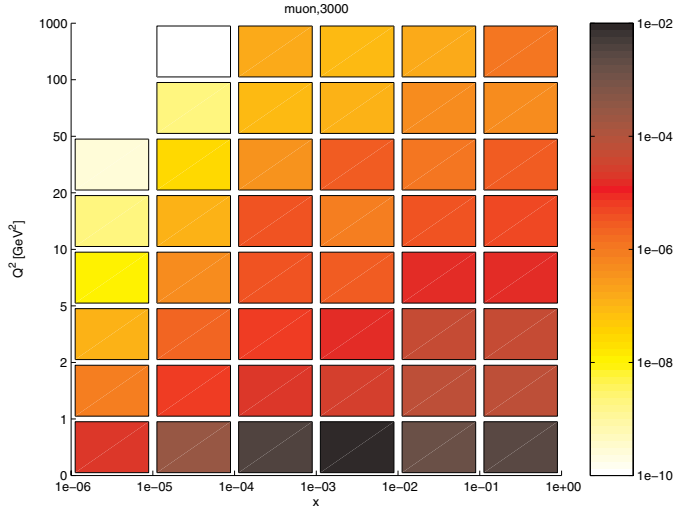

Fig. 17. Same as Fig. 16 but for muon-pair production

per bin in 30 days in the kinematic range $10^{-4} \leq x \leq 1$ and $0.2\,\mathrm{GeV}^2 \leq Q^2 \leq 1\,\mathrm{GeV}^2$ for electron-pair production and about a factor 10 less for muon-pair production at $\gamma = 3000$.

To test whether one sees a correlation between the energies of the "intermediate lepton" and the "spectator lepton", we present the cross section in barn as a function of the energies of the "intermediate lepton" E_{int} and of the "spectator lepton" E_{spec} in the rest system of the ion, that breaks up, in Fig. 18 for muon-pair production in a Pb–Pb collision for $\gamma = 3000$. The distribution is symmetric in the two energies and the region of energies up to 10 GeV is favored.

In Figs. 19 to 21 we present results from calculations including nuclear corrections to the parton distribution functions provided by Eskola et al. [17, 18] (referred to as EKS) and Frankfurt et al. [19, 20] (referred to as FGS). The calculations were performed in the kinematic range given by the sets, that is $2\,\mathrm{GeV} \leq Q \leq 100\,\mathrm{GeV}$. Because

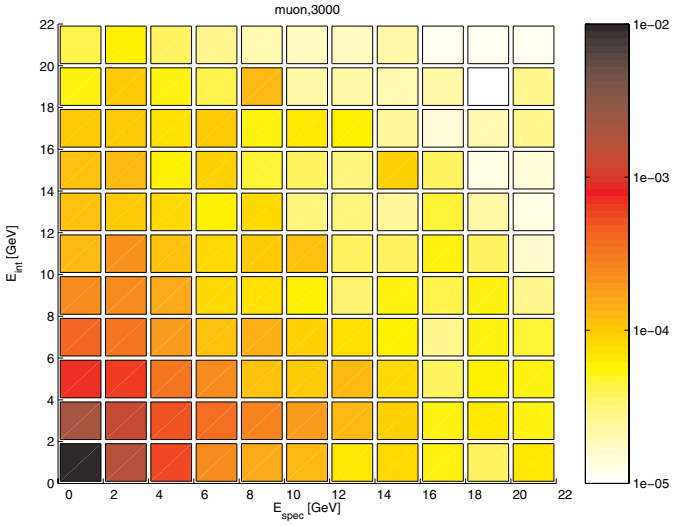

Fig. 18. Cross section in barn as a function of the energy E_{int} of the intermediate lepton and the energy E_{spec} of the spectator lepton for muon-pair production in a Pb–Pb collision at $\gamma = 3000$

a limitation of Q also limits the transverse momentum, we additionally apply a cut on the quark transverse momentum $p_{\perp\mathrm{quark}} > 2\,\mathrm{GeV}$.

We compare differential cross sections as a function of the transverse momentum of the "DIS lepton" $p_{\perp\mathrm{DIS}}$ (Fig. 19), Bjorken x (Fig. 20) and the rapidity of the "DIS lepton" Y_{DIS} (Fig. 21) of calculations using the EKS and FGS corrections with a calculation using free parton distribution functions, as they were used so far. The suppression of the cross section in the calculation using EKS is stronger than in the calculation using FGS, which can also be seen in a comparison of the correction factors to the structure function $R_{F_2} = \frac{F_2^A}{A \cdot F_2^{p(\mathrm{free})}}$ from the two sets as a function of Bjorken x at $Q = 3\,\mathrm{GeV}$ in Fig. 22.

The differential cross section as a function of the transverse momentum of the "DIS lepton" is not sensitive to the differences between the models, whereas one can clearly distinguish the models in the differential cross section as a function of the rapidity of the "DIS lepton". The effect of the reduction of the cross section due to the nuclear corrections is about 10%, which seems to be within the reach of the expected accuracy of measurement. In the differential cross section as a function of Bjorken x, one can see that $x \approx 10^{-3}$ is the relevant x-region.

For the ELA to be valid essentially two assumptions have to be fulfilled: First, the ELA is a high energy approximation, therefore all energies involved, especially the energy of the parent photon, should be much larger than the lepton mass ($E \gg m$). Second, the transverse momenta of the equivalent particles, the lepton pair in the ELA, should be small. The high energy assumption is obviously not fulfilled for muons in the collider frame at $\gamma = 100$, since there the parent photon energy is at most $\omega_{\max} = \gamma/R$ ($\approx 3000\,\mathrm{MeV}$) and will in most cases be much smaller. The fact that the high energy assumption does not hold in this case is most obvious in the differential cross sec-

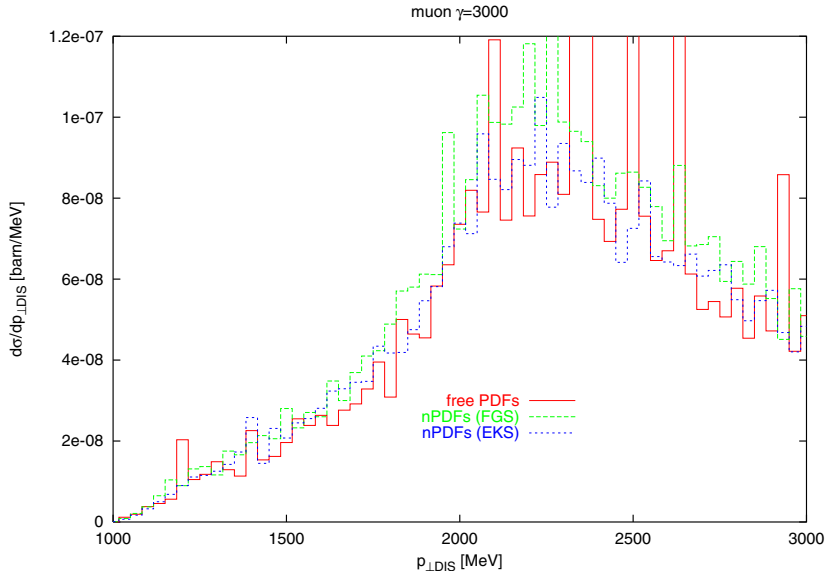

Fig. 19. Comparison of the differential cross sections as a function of the transverse momentum of the "DIS lepton" $\frac{d\sigma}{dp_\perp}$ for muon-pair production in a Pb–Pb collision for $\gamma = 3000$ in a full calculation using nuclear PDFs from the sets of Eskola et al. (EKS) and Frankfurt et al. (FGS) and in a calculation using free PDFs

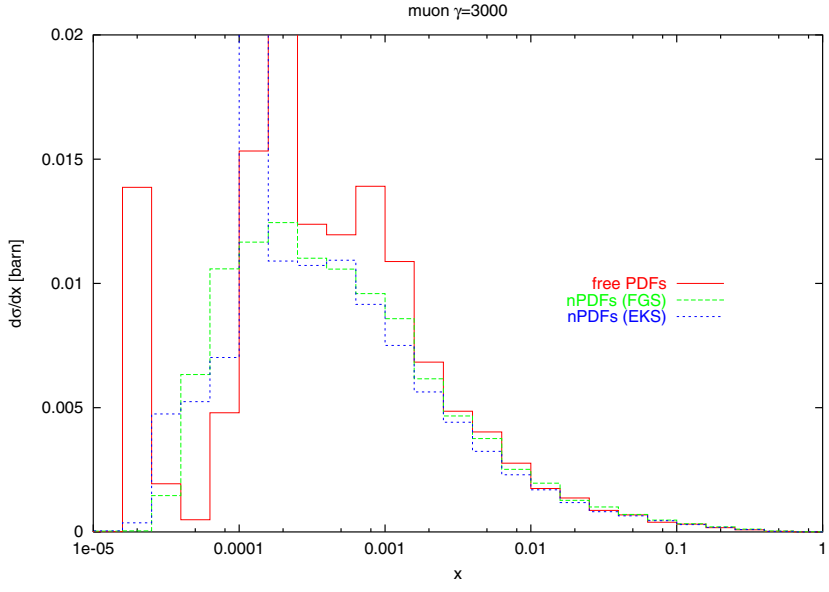

Fig. 20. Comparison of the differential cross sections as a function of Bjorken x, $\frac{d\sigma}{dx}$, for muon-pair production in a Pb–Pb collision for $\gamma = 3000$ in the full calculation using nuclear PDFs from the sets of Eskola et al. (EKS) and Frankfurt et al. (FGS) and in a calculation using free PDFs

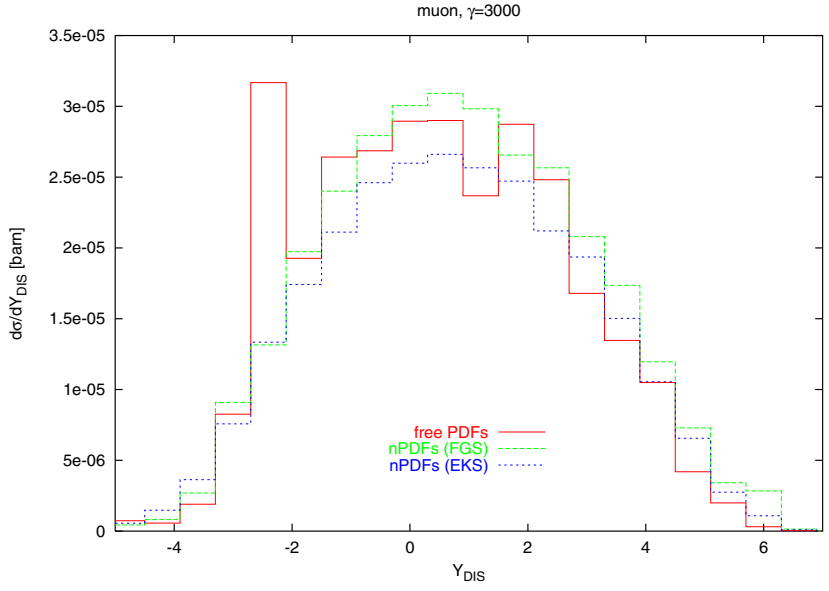

Fig. 21. Comparison of the differential cross sections as a function of the rapidity of the "DIS lepton" $\frac{d\sigma}{dY}$ for muon-pair production in a Pb–Pb collision for $\gamma = 3000$ in the full calculation using nuclear PDFs from the sets of Eskola et al. (EKS) and Frankfurt et al. (FGS) and in a calculation using free PDFs

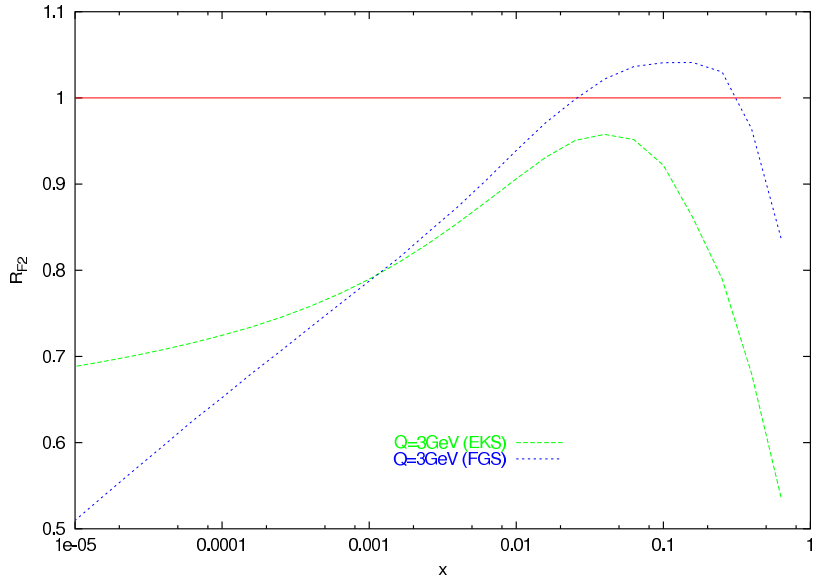

Fig. 22. Comparison of the ratios of the nuclear to free structure function of the nucleon $R_{F_2} = \frac{F_2^A}{A \cdot F_2^p}$ from Eskola et al. (EKS) and Frankfurt et al. (FGS) at $Q = 3\,\mathrm{GeV}$

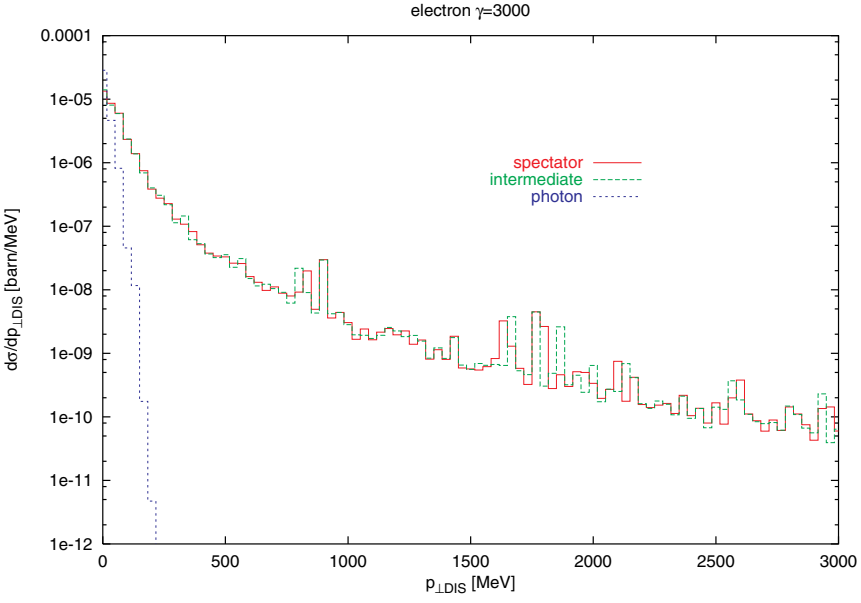

Fig. 23. Comparison of the differential cross sections as a function of the transverse momentum $\frac{\mathrm{d}\sigma}{\mathrm{d}p_\perp}$ of the "spectator lepton", the intermediate lepton and the photon from the elastic part of the process for electron-pair production in a Pb–p collision for $\gamma = 3000$ for the full calculation

tion as a function of the rapidity of the "DIS lepton". In Fig. 12 we show additionally a calculation using the ELA, where the equivalent lepton spectrum was derived in the collider frame. It can be seen that parts of the cross section are missing; therefore choosing a wrong frame would yield a too small total cross section. In all other plots we show those results of the calculation employing the ELA, where the equivalent lepton spectrum was derived in the target frame, since this is the more appropriate frame for such calculations.

Comparing the differential cross sections as functions of various kinematic variables from the EPA and the ELA with those of the full calculation, we see that the ELA, with the spectrum derived in the target frame, consistently overestimates the cross sections from the full calculation, while EPA works sufficiently well. To get an idea why the EPA succeeds in reproducing the results of the full calculation, while the ELA does not, we check the second approximation we made in the two methods. In the approximations we assume the equivalent particles (photons and leptons) to have small transverse momenta. To test this assumption we calculate in the full calculation the differential cross sections as a function of the transverse momenta of those particles, which are treated as equivalent particles in the approximations. These particles are the photon with momentum k from the elastic part of the process, the spectator lepton with momentum p_{spec} and the "DIS lepton", before it is scattered, which is, in the full calculation, the intermediate lepton $p_{\mathrm{int}} = p_{\mathrm{DIS}} - q$. As the equivalent particles are expected to proceed in forward direction, their transverse momentum should be close to zero for the approximations to be good. This is obviously the case for the photon as can be seen in Fig. 23. In contrast, the leptons have contributions to the cross section up to quite high transverse

momenta. This behavior explains why the equivalent lepton approximation is not as good as the equivalent photon approximation in this process. Large transverse momenta enlarge the denominator of the propagator, which leads to a smaller value for the cross sections in the full calculation than it is expected in the equivalent lepton approximation.

5 Conclusion

We identify two kinematic regions contributing about equally to the two-photon lepton-pair production in ultra-peripheral relativistic heavy ion collisions at large transverse momenta of at least one of the produced leptons. The contribution with one elastic and one deep inelastic interaction at the ions is especially interesting, because it provides a possibility to study the nuclear parton content. We calculated differential cross sections for this contribution as a function of various variables, in order to study in which kinematic regions one could expect viable amounts of events.

Furthermore we performed calculations including nuclear corrections to the PDFs provided by Eskola et al. and Frankfurt et al. and compare them to calculations using free PDFs. Applying the nuclear corrections the cross sections are suppressed in nearly all regions for FGS and in all regions for EKS.

In addition, we calculated differential cross sections of this process also in the equivalent photon and the equivalent lepton approximation and thus provide a test of the validity of the approximations. In conclusion, the cross sections calculated in the equivalent photon approximation resemble the ones from the full calculation quite well, whereas the equivalent lepton approximation consistently overestimates the cross sections. This is due to the fact that the assumption that the equivalent particles – the spectator lepton and the intermediate lepton in the full calculation – fly in forward direction is not fulfilled in this kind of process. There are contributions to the cross sections coming from the region of quite large transverse momenta of these particles. Nevertheless, the results confirm that the intuitive picture provided by the combination of both approximations, where one of the produced leptons is directly related to the large momentum transfer and therefore to the deep inelastic scattering, can still be applied.

Acknowledgements. We would like to thank Gerhard Baur and Mark Strikman for useful discussions and comments. This work was supported in part by the Schweizerischer Nationalfonds (SNF).

References

1. G. Baur et al., Phys. Rep. **364**, 359 (2002)
2. G. Racah, Nuovo Cimiento **14**, 93 (1937)
3. A. Alscher, K. Hencken, D. Trautmann, G. Baur, Phys. Rev. A **55**, 396 (1997) [nucl-th/9606011]
4. L.D. Landau, E.M. Lifshitz, Phys. Z. Sowjet Union **6**, 244 (1934)
5. M. Chen, P. Zerwas, Phys. Rev. D **12**, 187 (1975)
6. G. Baur, A. Leuschner, Eur. Phys. J. C **8**, 631 (1999) [hep-ph/9902245]
7. S.D. Drell, J.D. Walecka, Ann. Phys. **28**(1964)
8. C.A. Bertulani, G. Baur, Phys. Rep. **163**, 299 (1988)
9. C.A. Bertulani, S.R. Klein, J. Nystrand, nucl-ex/0502005
10. V.M. Budnev, I.F. Ginzburg, G.V. Meledin, V.G. Serbo, Phys. Rept. **15**, 181 (1974)
11. V.N. Baier, V.S. Fadin, V.H. Khoze, Nucl. Phys. B **65**, 381 (1973)
12. M.S. Chen, I.J. Muzinich, H. Terazawa, T.P. Cheng, Phys. Rev. D **7**, 3485 (1973)
13. W. Greiner, J. Reinhardt, Quantenelektrodynamik (Harri Deutsch, 1995)
14. W. Greiner, A. Schäfer, Quantenchromodynamik (Harri Deutsch, 1989)
15. F. Halzen, A.D. Martin, Quarks and leptons (John Wiley and sons, 1984)
16. www.phys.psu.edu/∼cteq/
17. K.J. Eskola, V.J. Kolhinen, C.A. Salgado, Eur. Phys. J. C **9**, 61 (1999) [hep-ph/9807297]
18. K.J. Eskola, V.J. Kolhinen, P.V. Ruuskanen, Nucl. Phys. B **535**, 351 (1998)
19. L. Frankfurt, V. Guzey, M. Strikman, hep-ph/0303022
20. L. Frankfurt, V. Guzey, M. McDermott, M. Strikman, JHEP **0202**, 027 (2002) [hep-ph/0201230]
21. E. Byckling, K. Kajantie, Particle kinematics (John Wiley and sons, 1973)
22. E.J. Williams, Phys. Rev. **45**, 729 (1934)
23. C.F. von Weizsäcker, Z. Phys. **88**, 612 (1934)
24. E. Fermi, Z. Phys. **29**, 315 (1924)